Acta Crystallographica Section D
Biological Crystallography
ISSN 0907-4449

Structure of the C2A domain of rabphilin-3A

Marianna Biadene,[a]‡ Pierre Montaville,[b]‡ George M. Sheldrick[a] and Stefan Becker[b]*

[a]Department of Structural Chemistry, University of Göttingen, Tammanstrasse 4, 37077 Göttingen, Germany, and [b]Department of NMR-based Structural Biology, Max-Planck-Institute for Biophysical Chemistry, Am Fassberg 11, 37077 Göttingen, Germany

‡ These authors contributed equally to this work.

Correspondence e-mail: sabe@nmr.mpibpc.mpg.de

Received 12 April 2006
Accepted 11 May 2006

PDB Reference: rabphilin-3A C2A domain, 2chd, r2chdsf.

Rabphilin-3A is a neuronal protein containing a C2-domain tandem. To date, only the structure of the C2B domain has been solved. The crystal structure of the Ca^{2+}-free C2A domain has been solved by molecular replacement and refined to 1.92 Å resolution. It adopts the classical C2-domain fold consisting of an eight-stranded antiparallel β-sandwich with type I topology. In agreement with its Ca^{2+}-dependent negatively charged membrane-binding properties, this C2 domain contains all the conserved acidic residues responsible for calcium binding. However, the replacement of a conserved aspartic acid residue by glutamic acid allows formation of an additional strong hydrogen bond, resulting in increased rigidity of calcium-binding loop 1. The electrostatic surface of the C2A domain consists of a large positively charged belt surrounded by two negatively charged patches located at both tips of the domain. In comparison, the structurally very similar C2A domain of synaptotagmin I has a highly acidic electrostatic surface, suggesting completely unrelated functions for these two C2A domains.

1. Introduction

Rabphilin-3A is a 78 kDa cytosolic protein that is almost exclusively expressed in neurons and neuroendocrine cells. As a putative Rab effector, a role for rabphilin-3A in synaptic function, more specifically in the calcium-regulated exocytotic and endocytotic processes, has been suggested by many studies in isolated synapses and cultured cells (Chung *et al.*, 1995; Arribas *et al.*, 1997; Komuro *et al.*, 1996; Burns *et al.*, 1998; Ohya *et al.*, 1998). However, recent studies of rabphilin mutants in mouse and *Caenorhabditis elegans* showed that rabphilin is largely dispensable for calcium-triggered neurotransmitter release (Staunton *et al.*, 2001; Schluter *et al.*, 1999). Other studies have claimed a direct interaction of rabphilin-3A with the SNARE-complex component SNAP25 (Tsuboi & Fukuda, 2005) and a possible potentiation function for the SNARE complex independently of Rab3 (Staunton *et al.*, 2001). Thus, the exact biological role of rabphilin-3A still remains to be elucidated; for example, rabphilin-3A has also been shown to bind α-actinin (*via* its N-terminal domain; Kato *et al.*, 1996; Baldini *et al.*, 2005) and β-adducin (*via* its C2 domains; Miyazaki *et al.*, 1994), two components of the cytoskeleton.

The N-terminal part of rabphilin-3A consists of a cysteine-rich Zn^{2+}-binding domain which interacts with the small GTPases Rab3a and Rab27 (Fukuda, 2003; McKiernan *et al.*, 1996). The C-terminal portion of rabphilin-3A is formed by a tandem of C2 domains, namely C2A and C2B, that are

Table 1
Data statistics for the C2A domain of rabphilin-3A.

Values in parentheses are for the highest resolution shell (1.95–1.92 Å, corresponding to 439 observations).

Space group	$P2_12_12_1$
Unit-cell parameters (Å, °)	a = 37.84 (7), b = 39.16 (2), c = 88.95 (4), $\alpha = \beta = \gamma = 90$
Resolution range (Å)	44.41–1.92
No. of observations	65418
No. of unique reflections	10435
Redundancy	6.13 (2.74)
$\langle I\rangle/\sigma(I)$	19.11 (3.09)
Completeness (%)	97.8 (92.6)
$R_{\rm int}$ (%)	5.15 (28.37)

responsible for the Ca^{2+}- and phospholipid-binding properties of rabphilin. The structure of the C2B domain has been solved by NMR (Ubach *et al.*, 1999). The Rab-binding domain and the C2-domain tandem are connected by a long (about 200 residues) variable linker of unknown structure and function.

C2 domains are ubiquitous protein modules consisting of approximately 130 residues (Nalefski & Falke, 1996). They are generally involved in signal transduction or membrane trafficking. All C2 domains share a common fold consisting of an eight-stranded antiparallel β-sandwich, all strands being connected by variable loops. Two main topologies have been described for these domains, namely the type I topology, first described for the synaptotagmin C2A domain, and the type II topology found originally in the phosphoinositide-specific phospholipase Cδ1 (for a review, see Rizo & Sudhof, 1998). In a number of C2-domain-harbouring proteins these domains appear to be involved in targeting to biological membranes. They generally present a Ca^{2+}-binding pocket in which two to three Ca^{2+} ions can be found. An intracellular Ca^{2+}-concentration increase triggers the localization of these proteins to anionic phospholipid-enriched membrane subdomains through a Ca^{2+}-bridging mechanism (Verdaguer *et al.*, 1999).

To date, apart from the linker region which has no predicted structural features, the C2A domain of rabphilin-3A remains the only module which has not been structurally characterized. The modular C2-domain tandem structure characteristic of the synaptotagmin protein family is essential for the function of these proteins owing to the functional cooperativity shown by these two consecutive C2 domains (Bai & Chapman, 2004). Therefore, elucidating the structural features of the C2A domain of rabphilin-3A will also help to highlight the functional properties of this protein. With this aim, we report here the X-ray structure of this domain determined at 1.92 Å resolution.

2. Material and methods

2.1. Cloning, expression and purification

A cDNA coding for the C2A domain of rat rabphilin-3A (Glu371–Ile510) was cloned into the *Bam*HI and *Eco*RI restriction sites of pGEX-2T (Novagen, Madison, USA) in order to produce GST-tagged recombinant protein in *Escherichia coli* BL21. From the cloning, the protein obtained after thrombin cleavage contains two additional N-terminal residues Gly-Ser. After induction with 1 m*M* IPTG, the fusion protein was expressed overnight at 290 K. After lysis of the

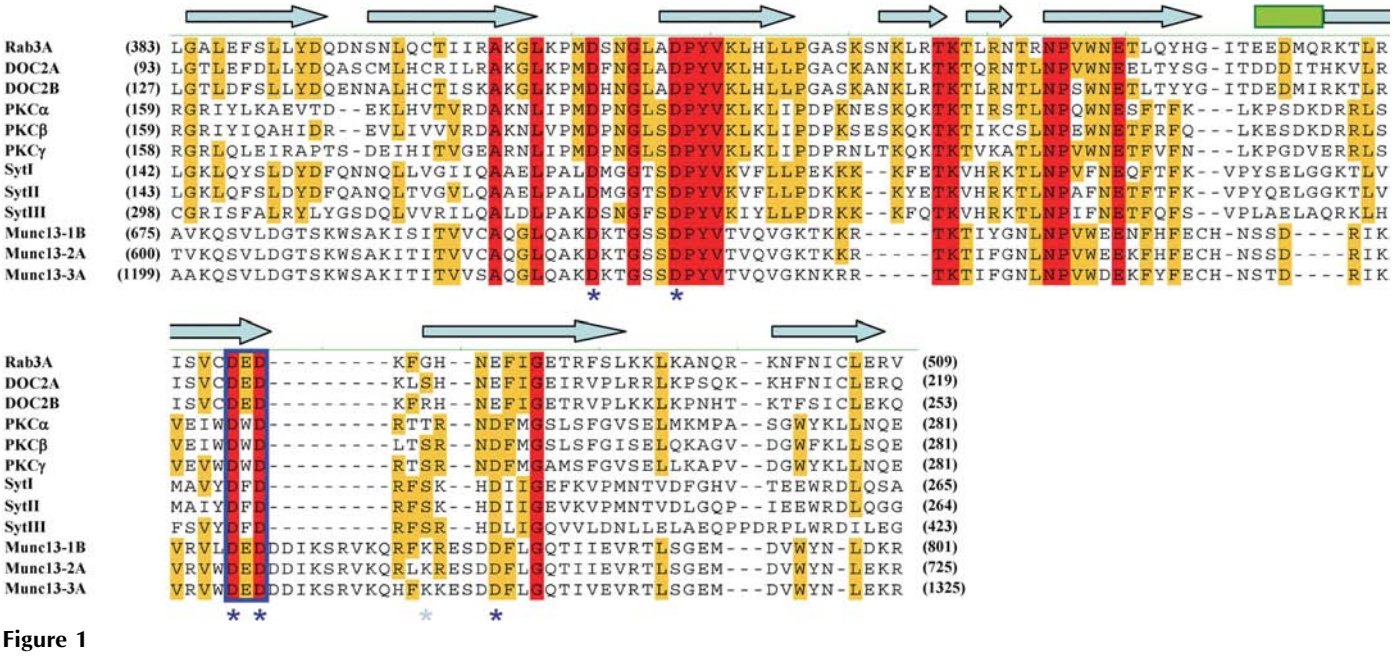

Figure 1
Sequence alignment of several C2 domains: alignment of C2A domains (C2B for Munc13-1) of protein sequences from rat. From top to bottom: rabphilin-3A, DOC2A, DOC2B, protein kinases Cα, Cβ and Cγ, synaptotagmins I, II and III, Munc13-1, Munc13-2 and Munc13-3. Red boxes highlight identical residues; orange boxes highlight conserved residues. This alignment was performed in *Vector NTI*. The blue box shows the DED motif present in rabphilin, DOC2A/B and Munc13-1/2/3 proteins. The secondary-structure elements were drawn according to the rabphilin-3A C2A structure: β-sheets are represented by blue arrows and the α-helix by a green box. Dark blue asterisks represent the conserved Ca^{2+}-binding residues described for the C2A domain of synaptotagmin I and the light blue asterisk corresponds to the only non-conserved Ca^{2+}-binding residue in the presented structure.

Table 2
Refinement statistics for *SHELXL* refinement.

R_{work} (%)	19.3
R_{free} (%)	24.0
No. of protein atoms per ASU	1056
No. of non-protein atoms	72
R.m.s.d. bond lengths (Å)	0.005
R.m.s.d. angle distances (Å)	0.023
Average B (Å^2)	27.7
Ramachandran plot statistics	
Residues in most favoured regions (%)	83.5
Residues in additional allowed regions (%)	15.7
Residues in disallowed regions (%)	0.9

resuspended bacterial pellet, the soluble fusion protein was purified by affinity chromatography on glutathione Sepharose resin (Amersham Biosciences) and the GST tag was removed on-column by thrombin cleavage. The protein was further purified by anion-exchange chromatography on a HiTrap SP-Sepharose column (Amersham Biosciences). Size-exclusion chromatography (Superdex 75 16/60) in a buffer containing 10 m*M* HEPES pH 7.0, 150 m*M* NaCl, 1 m*M* DTT was performed as the last step in the purification protocol. A final yield of 5–7 mg was typically obtained from 1 l LB medium.

2.2. Crystallization and data collection

For crystallization, the protein was concentrated in 10 m*M* HEPES pH 7.0, 150 m*M* NaCl, 1 m*M* DTT to a final concentration of 10 mg ml^{-1}. The reservoir solution contained 25%(*w*/*v*) PEG 4000, 0.1 *M* ammonium sulfate and 0.1 *M* sodium acetate pH 4.6. Drops were set up in 96-well Greiner low-profile plates using a Mosquito robot (TTP Labtech). 100 nl protein solution was mixed with 100 nl reservoir solution. Crystals appeared overnight and grew for about two weeks. Scaling up these conditions in 24-well plates using the hanging-drop method was not successful.

Crystals were mounted in Hampton loops using 30%(*v*/*v*) glycerol as cryo-protectant and were flash-cooled in a stream of liquid nitrogen. Data were collected in-house in fine-sliced mode (0.2°) using a Bruker rotating-anode generator, Cu $K\alpha$ radiation, Osmic focusing mirrors and a Bruker *SMART*6000 4K CCD detector placed at a distance of 7 cm. The exposure time was 70 s for the low-resolution pass and 120 s for high-resolution data collection. The best crystal diffracted to 1.82 Å. The data were indexed with the Bruker program *PROTEUM*, integrated with the Bruker program *SAINT* and scaled with the Bruker program *SADABS*. After scaling, the statistics were obtained and the space-group determination was performed with the Bruker program *XPREP*. In light of the statistics, the data were cut at 1.92 Å. The crystals belong to the orthorhombic space group $P2_12_12_1$, with unit-cell parameters a = 37.84 (7), b = 39.16 (2), c = 88.95 (4) Å, $\alpha = \beta = \gamma = 90°$. There is one molecule per asymmetric unit and the solvent content of the crystals is 39.8%, with a Matthews coefficient of 2.1 Å^3 Da^{-1}. The data statistics are shown in Table 1.

2.3. Structure determination and refinement

The structure was solved by molecular replacement using data to 2.5 Å. The search model was based on the structure of the C2A domain of synaptotagmin I (PDB code 1rsy; residues 140–265; Sutton *et al.*, 1995), which has a sequence identity of 40% (Fig. 1). The final search model was generated by replacing the residues that differed by alanines. Using this mixed model and the program *Phaser* (McCoy *et al.*, 2005), a solution was found. After a rigid-body refinement in *REFMAC* (R_{work} = 53%, R_{free} = 54%; Murshudov *et al.*, 1997), the program *RESOLVE* was employed for density modification, reducing the model bias with the prime-and-switch procedure (Terwilliger, 2000), and for model building (Terwilliger, 2002). The partial model obtained from *RESOLVE* contained 111 correctly placed residues (104 of them with side chains built) out of 127 (R_{work} = 36%, R_{free} = 38%). Tracing and rebuilding was continued using the graphics program *COOT* (Emsley & Cowtan, 2004) alternating with refinement in *REFMAC* (first isotropic minimization and then TLS refinement considering the whole protein as a single domain). The final model from the *REFMAC* refinement has an R_{work} of 19.6% and an R_{free} of 26.0% and contains 127 residues, 66 water molecules and one glycerol molecule. The

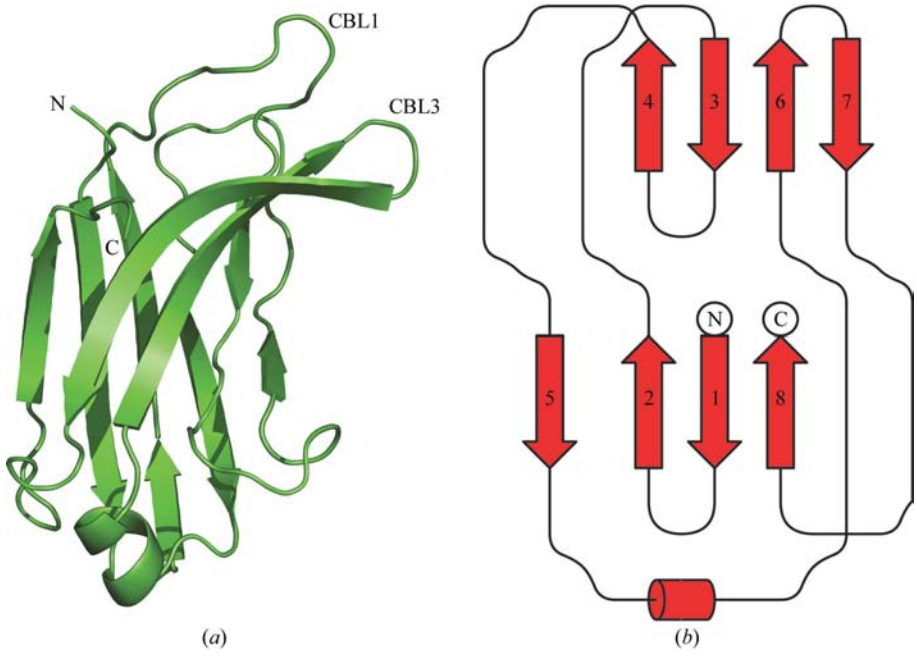

Figure 2
Overall structure of the C2A domain of rabphilin-3A. (*a*) Cartoon drawing showing the common eight-stranded antiparallel β-sandwich. (*b*) Topology diagram (made with the program *TOPDRAW*; Bond, 2003).

model of the last *REFMAC* refinement was further refined using *SHELXL* (Sheldrick & Schneider, 1997). The version of *SHELXL* used was a test version with restraints that mimic a TLS refinement. An R_{work} of 19.31% and an R_{free} of 23.97% were obtained. Analysis with *PROCHECK* (Laskowski *et al.*, 1993) shows that 83.5% of the residues are in the most favoured regions, 15.7% are in the additional allowed regions and 0.9% are in the disallowed region (residue Lys432; the electron density of this residue is not well defined, in line with its relatively high B value of 45 Å^2). The statistics for the *SHELXL* refinement are shown in Table 2.

3. Results and discussion

3.1. Structure description

The refined crystal structure of the C2A domain of rabphilin-3A includes 127 residues (Tyr382–Val509; Fig. 2*a*). The structure consists of a compact β-sandwich formed by two four stranded β-sheets, one small helix and three loops at the top and the bottom of the sandwich, respectively. The C2A domain has the topology I found in all other C2 domains of synaptotagmin proteins (Fig. 2*b*).

Soaking the crystals with Ca^{2+} resulted in a dramatic loss of crystal quality. Screening for crystallization conditions with Ca^{2+}-containing reservoir solutions did not result in a Ca^{2+}-bound crystal form. Although Ca^{2+} has not been found in the structure, the loops located in the Ca^{2+}-binding region [residues 411–421 (CBL1) and 474–484 (CBL3)] are well ordered: for CBL1 the C^{α} atoms have an average B factor of 19 Å^2, while for CBL3 the average B factor is 23 Å^2. The residues normally involved in Ca^{2+} binding are in the calcium-free conformation (Fig. 3), similar to that described in the synaptotagmin I C2A domain crystal structure (Sutton *et al.*, 1995). The quality of the electron density at the N-terminal end of the fourth β-strand was not good enough to build the side chains of the residues, but the main chain could be unambiguously traced in this region. One glycerol molecule, presumably introduced by soaking with glycerol for cryoprotection, has been modelled near Asn481, Lys423 and Lys410 of a symmetry-related C2A molecule. The glycerol molecule is in the same position as a phosphate found in the structure of synaptotagmin III (Sutton *et al.*, 1999). As sodium sulfate was a component of the crystallization condition, we also tried to place a sulfate ion instead of glycerol into this electron density, but this resulted in very high B values, suggesting that glycerol was the better choice. Double conformations were modelled for six of the 127 residues (Cys401, His425, Asp434, Lys439, Asn450 and Arg469). For four residues (Gln460, Glu461, Lys492 and Lys495) only part of the side chain has been modeled. A *cis*-peptide bond was detected between Leu427 and Pro428.

3.2. Comparison with structurally similar C2 domains

The crystal structure of the rabphilin-3A C2A domain was superimposed on the structures of the C2A domains of synaptotagmin I (PDB code 1rsy; Sutton *et al.*, 1995), synaptotagmin III (PDB code 1dqv; Sutton *et al.*, 1999), protein kinase Cβ (PDB code 1a25; Sutton & Sprang, 1998) and protein kinase Cα (PDB code 1dsy; Verdaguer *et al.*, 1999) (Fig. 4) using the program *SSM* within *COOT* (Krissinel & Henrick, 2004). The r.m.s. deviations between the structure described here and the C2A domains of synaptotagmin I and synaptotagmin III are 1.21 and 1.81 Å, respectively. The r.m.s. deviations from the C2 domains of protein kinase Cα and protein kinase Cβ are also quite small (1.44 and 1.45 Å, respectively).

The structure of the C2A domain of synaptotagmin I, which had been successfully used as a search model for molecular replacement, is indeed very similar. The major differences are visible in CBL1 and CBL3, which connect strands β2 and β3 and strands β6 and β7, respectively. CBL1 is flipped by 20° and rotated by 90° compared with CBL1 of the homologous C2 domains (Fig. 4), but in all three structures it is well ordered (B values of 15–20 Å^2). One consequence of these structural changes is a significant shift of the position of residue Asp413 compared with the equivalent residue Asp172 found in the C2A domain of synaptotagmin I. The longer side chain of Glu482 compared with the conserved aspartate found in other C2 domains (Asp238 in the case of synaptotagmin I) facilitates a hydrogen bond between its carboxylic moiety and the backbone NH of Asp413 located in CBL1 (Fig. 5). Of the Ca^{2+}-binding residues commonly found in type I C2 domains, the only residue which is not conserved in the C2A domain of rabphilin-3A is Gly479 (Fig. 1), which is structurally homologous to Ser235 located in CBL3 of the C2A domain of synaptotagmin I (Shao *et al.*, 1998).

The structure of the C2A domain of synaptotagmin III also strongly resembles the C2A domain presented in this study. The quality of the electron density of the loop between β3 and β4 is very limited in all three structures: in 1dqv it is disordered with very high B values (90–100 Å^2), in 1rsy four of the residues have zero occupancy (Lys189, Lys190, Lys191 and Lys192) and in the structure described here it is also disordered.

3.3. Comparison of electrostatic surfaces

The electrostatic potential, mapped onto the molecular surface of the C2A domain of rabphilin, consists of a positively charged belt surrounded by two localized negative patches (Fig. 6). The first negative patch is located in the calcium-binding region. It contains all the acidic residues, as described for the synaptotagmin I C2A or protein kinase Cα C2 domains, that are necessary to chelate two or three Ca^{2+} ions. The Ca^{2+} binding reverses this acidic character. This electrostatic switch is strictly required in order to approach the anionic phospholipid subdomains (Murray & Honig, 2002). Previous studies showed that the rabphilin-3A C2A domain is able to interact with phospholipids in a Ca^{2+}-dependent manner (Chung *et al.*, 1998), suggesting that these conserved residues are indeed able to bind Ca^{2+}. The second negative patch sits at the tip located at the opposite end of the domain relative to the Ca^{2+}-binding region (CBR). The acidic residues

involved are located in two structure elements, namely the short helix *A* connecting strands $\beta5$ and $\beta6$ and the turn between strands $\beta1$ and $\beta2$. This region might be involved in the interaction of the C2A domain with an as yet unidentified partner.

The C2A domain of rabphilin-3A forms part of a C2-domain tandem. The electrostatic surfaces of both the C2A and the C2B domains show a strongly positive character, contrary to the synaptotagmin I C2-domain tandem, where the C2A domain is negatively charged and the C2B domain is highly basic. This observation is suggestive of different roles for both C2A domains and thus for the C2-domain tandems of rabphilin-3A and synaptotagmin I.

The residues from the polybasic region of β-strand 4 of the C2 domain of protein kinase Cα (PKCα) that have been reported to be responsible for phosphatidylinositol-4,5-bisphosphate (PIP2) binding (Corbalan-Garcia *et al.*, 2003) are conserved in the rabphilin-3A C2A domain. It has been shown that the C2A domain of rabphilin-3A is able to specifically bind PIP2 in the presence of Ca^{2+} (Chung *et al.*, 1998). In the rabphilin-3A C2A domain, these conserved amino acids form part of the large basic belt in the presented structure, whereas they were involved in a restricted positive patch in the case of PKCα. In addition to PIP2 binding, it has been shown that this polybasic region of PKCα is involved in the proper subcellular localization of the whole protein upon calcium signalling. It will be interesting to study whether this feature is essential for the role of the rabphilin C2A domain in rabphilin function.

3.4. DED motif

A recent study pointed out the high calcium sensitivity of the C2A domain of DOC2A and DOC2B and hypothesized

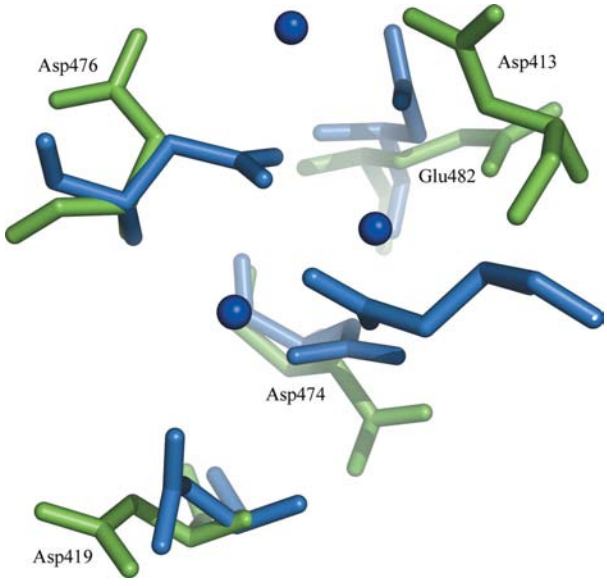

Figure 3
Residues in the Ca^{2+}-binding region: the residues of the C2A domain of rabphilin-3A are coloured green and the residues of synaptotagmin I and the Ca^{2+} ions present in that structure (PDB code 1byn) are coloured blue.

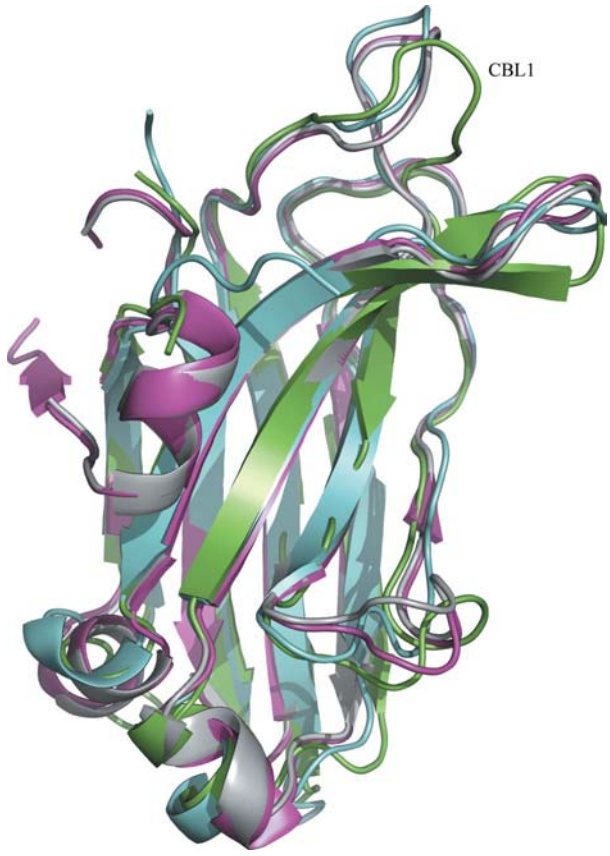

Figure 4
Superposition of C2 domains: the C2A domains of rabphilin-3A (green) and synaptotagmin I (cyan) and the C2 domains of protein kinase Cα (magenta) and protein kinase Cβ (grey).

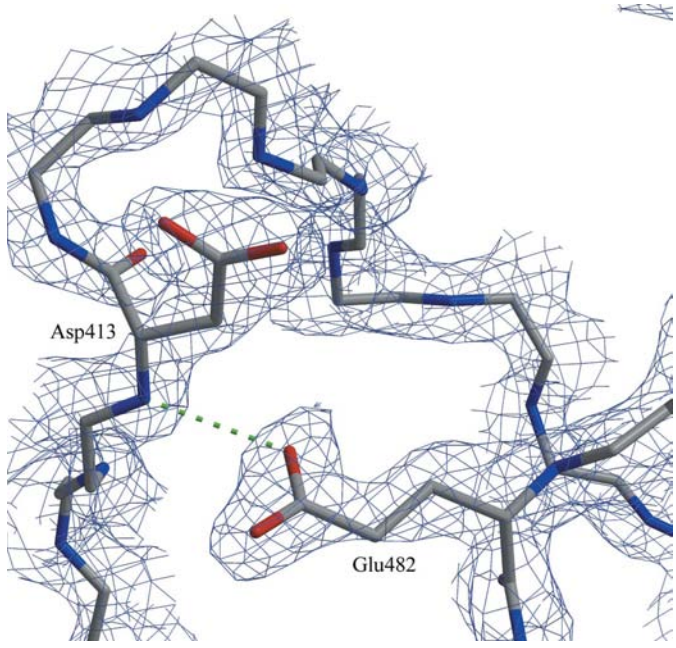

Figure 5
σ_A-weighted electron-density map (contoured at 1σ) of the loop between residues 411 and 421 and the strand from residues 482 to 484. The density for some side chains has been omitted for clarity. The hydrogen bond between Asp413 and Glu482 is indicated by a dashed line.

that this feature could be linked to a DED motif found in strand β6 (Groffen *et al.*, 2006). In the case of topology I type C2 domains, this motif has been found in the C2 domains of DOC2A/B, MUNC13 and rabphilin-3A (Nalefski & Falke, 1996). The glutamic acid positioned between the two highly conserved aspartic acids that are involved in the normal calcium-binding sites is usually found to be a tyrosine or a phenylalanine in other C2 domains. The structure presented here is the first C2-domain structure containing this DED motif. The Glu475 side chain points towards the concave side of the structure, opposite the Ca^{2+}-binding region. Its carboxylic acid group is located near the conserved residue Asp419 and close to the hydroxyl group of Thr440, resulting in a negatively charged patch (Fig. 7). The potential role of this atypical acidic residue might be involvement in a new calcium-binding site or modification of the ability of CBL3 to bind Ca^{2+}. Further investigations will be necessary to describe the exact role of this specific motif.

4. Conclusions and perspectives

The crystal structure of the Ca^{2+}-free C2A domain of rabphilin has been determined at 1.92 Å resolution. It has a classical type I eight-stranded antiparallel β-sandwich structure as found in synaptotagmin or PKCα C2 domains. It contains all the acidic residues responsible for Ca^{2+} binding, in agreement with its calcium-dependent membrane-binding properties. Its electrostatic surface is highly basic, similar to the juxtaposed C2B domain of rabphilin-3A. Other studies have indicated that Ca^{2+} binding to C2 domains does not induce large conformational changes and that the Ca^{2+}-binding properties of a specific C2 domain cannot readily be inferred from its primary sequence (Dai *et al.*, 2004). Thus, slight structural modifications may account for changes in functional specificities from one C2 domain to another. Two specific structural features related to deviations from the consensus sequence have been found in the C2A domain of rabphilin-3A: a modification in the position of the Ca^{2+}-binding loop 1 that promotes a significant deviation of a conserved Ca^{2+}-binding residue (Asn413) and Glu475, which creates a

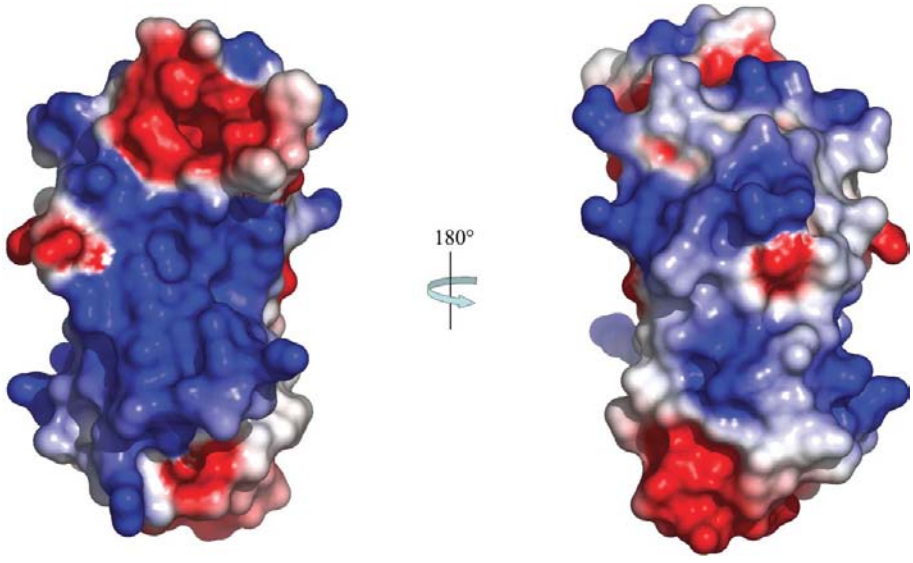

Figure 6
Electrostatic potential of the rabphilin-3A C2A-domain surface. The Poisson–Boltzmann electrostatic potential was calculated and mapped onto the molecular surface of the C2A domain. The left view shows the concave site of the C2A domain; the Ca^{2+}-binding region is at the top. The right view shows the other side of the β-sandwich. The computational results for the electrostatic surface were obtained using *DelPhi* (Honig & Nicholls, 1995) and the graphical displays were produced using *PyMOL* (DeLano, 2002).

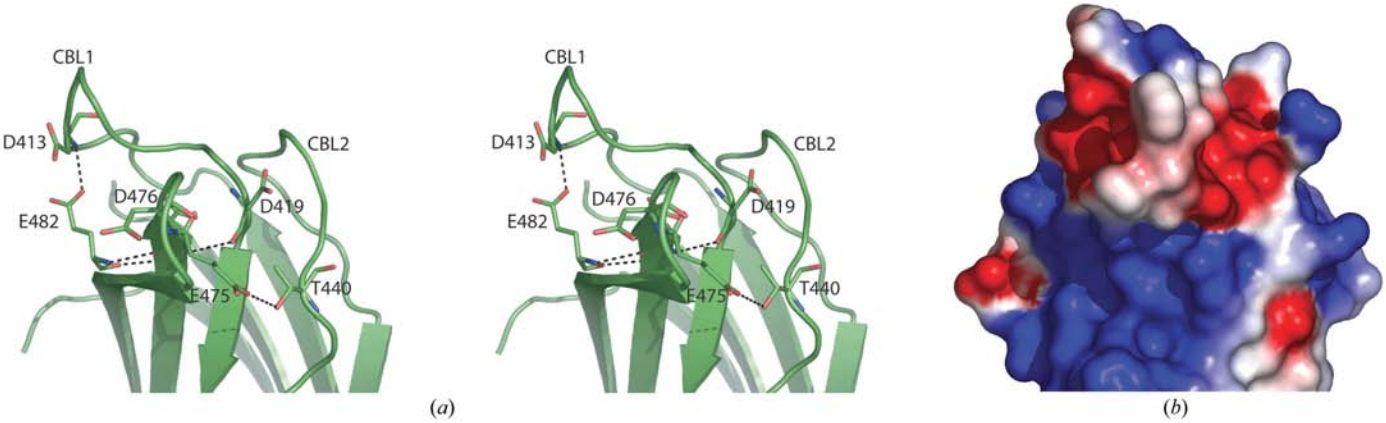

Figure 7
Influence of the DED motif on the electrostatic potential surface close to the calcium-binding region. (*a*) Stereoview of the calcium-binding region of the C2A domain of rabphilin-3A. CBL1 and CBL2 are labelled. CBL3 is oriented perpendicular to the plane of the figure. The residues Glu482, Asp413, Asp476 and Asp419 are the conserved residues involved in Ca^{2+} binding (in this view Asp474 lies behind β-strand 6). The residue Glu475 from the DED motif forms hydrogen bonds with the Thr440 side chain and the Asp419 backbone O atom. (*b*) Electrostatic surface mapped onto the same view of the C2A domain as shown in (*a*). The close proximity of the residue Glu475, Thr440 and Asp419 creates a new negative patch next to the calcium-binding region. The electrostatic surface was calculated as described for Fig. 6.

localized negative patch in close proximity to the Ca^{2+}-binding region. Further investigations are in progress to determine the relationship between the structural particularities of the C2 domain described in this work and its specific biophysical properties.

We thank Kamila Budzyn for expert technical help. We thank Professor C. Griesinger for generous support. We are grateful to the DFG and Funds der Chemische Industrie for support. This work was supported by the Max Planck Society.

References

Arribas, M., Regazzi, R., Garcia, E., Wollheim, C. B. & De Camilli, P. (1997). *Eur. J. Cell Biol.* **74**, 209–216.
Bai, J. & Chapman, E. R. (2004). *Trends Biochem. Sci.* **29**, 143–151.
Baldini, G., Martelli, A. M., Tabellini, G., Horn, C., Machaca, K., Narducci, P. & Baldini, G. (2005). *J. Biol. Chem.* **280**, 34974–34984.
Bond, C. S. (2003). *Bioinformatics*, **19**, 311–312.
Burns, M. E., Sasaki, T., Takai, Y. & Augustine, G. J. (1998). *J. Gen. Physiol.* **111**, 243–255.
Chung, S. H., Song, W. J., Kim, K., Bednarski, J. J., Chen, J., Prestwich, G. D. & Holz, R. W. (1998). *J. Biol. Chem.* **273**, 10240–10248.
Chung, S. H., Takai, Y. & Holz, R. W. (1995). *J. Biol. Chem.* **270**, 16714–16718.
Corbalan-Garcia, S., Garcia-Garcia, J., Rodriguez-Alfaro, J. A. & Gomez-Fernandez, J. C. (2003). *J. Biol. Chem.* **278**, 4972–4980.
Dai, H., Shin, O. H., Machius, M., Tomchick, D. R., Sudhof, T. C. & Rizo, J. (2004). *Nature Struct. Mol. Biol.* **11**, 844–849.
DeLano, W. L. (2002). *The PyMOL Molecular Graphics System.* http://www.pymol.org.
Emsley, P. & Cowtan, K. (2004). *Acta Cryst.* D**60**, 2126–2132.
Fukuda, M. (2003). *J. Biol. Chem.* **278**, 15373–15380.
Groffen, A. J., Friedrich, R., Brian, E. C., Ashery, U. & Verhage, M. (2006). *J. Neurochem.* **97**, 818–833.
Honig, B. & Nicholls, A. (1995). *Science*, **268**, 1144–1149.
Kato, M., Sasaki, T., Ohya, T., Nakanishi, H., Nishioka, H., Imamura, M. & Takai, Y. (1996). *J. Biol. Chem.* **271**, 31775–31778.
Komuro, R., Sasaki, T., Orita, S., Maeda, M. & Takai, Y. (1996). *Biochem. Biophys. Res. Commun.* **219**, 435–440.
Krissinel, E. & Henrick, K. (2004). *Acta Cryst.* D**60**, 2256–2268.
Laskowski, R. A., MacArthur, M. W., Moss, D. S. & Thornton, J. M. (1993). *J. Appl. Cryst.* **26**, 283–291.
McCoy, A. J., Grosse-Kunstleve, R. W., Storoni, L. C. & Read, R. J. (2005). *Acta Cryst.* D**61**, 458–464.
McKiernan, C. J., Stabila, P. F. & Macara, I. G. (1996). *Mol. Cell. Biol.* **16**, 4985–4995.
Miyazaki, M., Shirataki, H., Kohno, H., Kaibuchi, K., Tsugita, A. & Takai, Y. (1994). *Biochem. Biophys. Res. Commun.* **205**, 460–466.
Murray, D. & Honig, B. (2002). *Mol. Cell*, **9**, 145–154.
Murshudov, G. N., Vagin, A. A. & Dodson, E. J. (1997). *Acta Cryst.* D**53**, 240–255.
Nalefski, E. A. & Falke, J. J. (1996). *Protein Sci.* **5**, 2375–2390.
Ohya, T., Sasaki, T., Kato, M. & Takai, Y. (1998). *J. Biol. Chem.* **273**, 613–617.
Rizo, J. & Sudhof, T. C. (1998). *J. Biol. Chem.* **273**, 15879–15882.
Schluter, O. M., Schnell, E., Verhage, M., Tzonopoulos, T., Nicoll, R. A., Janz, R., Malenka, R. C., Geppert, M. & Sudhof, T. C. (1999). *J. Neurosci.* **19**, 5834–5846.
Shao, X., Fernandez, I., Sudhof, T. C. & Rizo, J. (1998). *Biochemistry*, **37**, 16106–16115.
Sheldrick, G. M. & Schneider, T. R. (1997). *Methods Enzymol.* **277**, 319–343.
Staunton, J., Ganetzky, B. & Nonet, M. L. (2001). *J. Neurosci.* **21**, 9255–9264.
Sutton, R. B., Davletov, B. A., Berghuis, A. M., Sudhof, T. C. & Sprang, S. R. (1995). *Cell*, **80**, 929–938.
Sutton, R. B., Ernst, J. A. & Brunger, A. T. (1999). *J. Cell. Biol.* **147**, 589–598.
Sutton, R. B. & Sprang, S. R. (1998). *Structure*, **6**, 1395–1405.
Terwilliger, T. C. (2000). *Acta Cryst.* D**56**, 965–972.
Terwilliger, T. C. (2002). *Acta Cryst.* D**58**, 1937–1940.
Tsuboi, T. & Fukuda, M. (2005). *J. Biol. Chem.* **280**, 39253–39259.
Ubach, J., Garcia, J., Nittler, M. P., Sudhof, T. C. & Rizo, J. (1999). *Nature Cell. Biol.* **1**, 106–112.
Verdaguer, N., Corbalan-Garcia, S., Ochoa, W. F., Fita, I. & Gomez-Fernandez, J. C. (1999). *EMBO J.* **18**, 6329–6338.